Electronic Supplementary Material (ESI) for Polymer Chemistry

Polymer bottlebrushes with redox responsive backbone feel the heat: Synthesis and characterization of dual responsive poly(ferrocenylsilane)s with PNIPAM side chains

Edit Kutnyanszky, Mark A. Hempenius and G. Julius Vancso*

[0]Materials Science and Technology of Polymers, MESA+ Institute for Nanotechnology, University of Twente, P.O. Box 217, 7500 AE Enschede, The Netherlands. Fax: +31 53 489 3823; Tel: +31 53 489 2974; E-mail: g.j.vancso@utwente.nl

1 Synthesis of Bb1 , Bb2 , Bb3

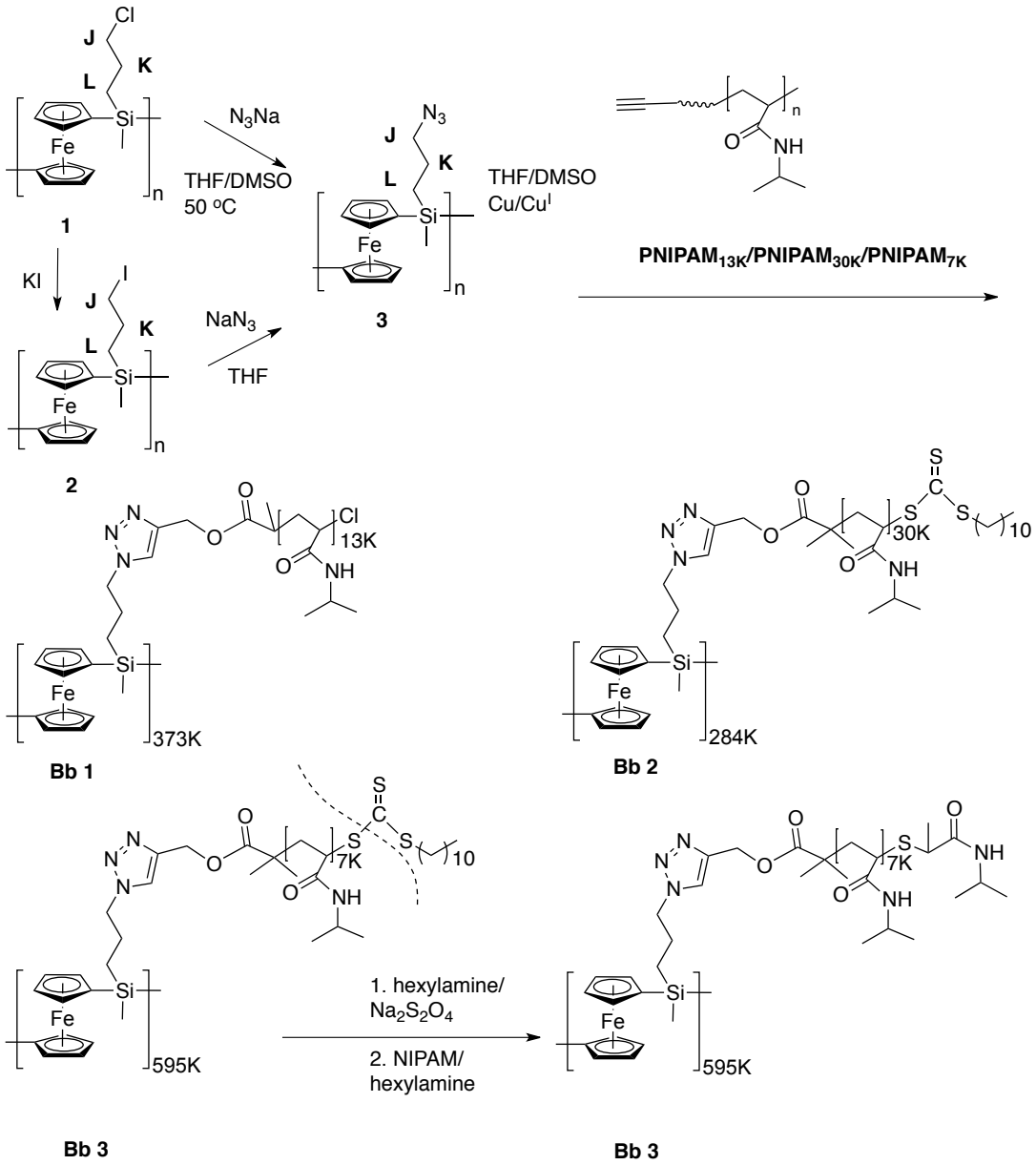

Scheme S1 Synthesis of bottlebrushes (**Bb1** , **Bb2** , **Bb3**) via click chemistry.

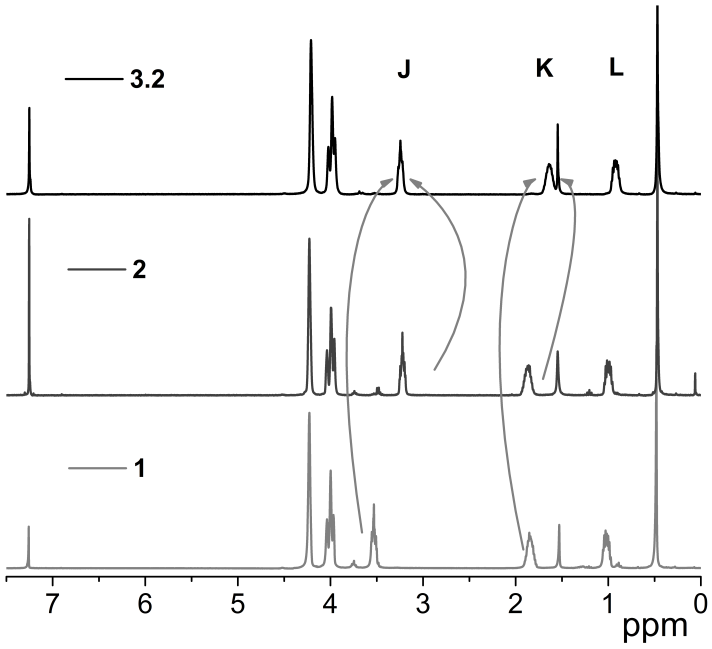

Figure S1 ^{1}H NMR spectra of **1**, **2** and **3**. Side group conversions are evident from the shift of the peaks belonging to the pendant groups attached to Si. For guidance to the symbols **J**, **K** and **L** see Scheme S1.

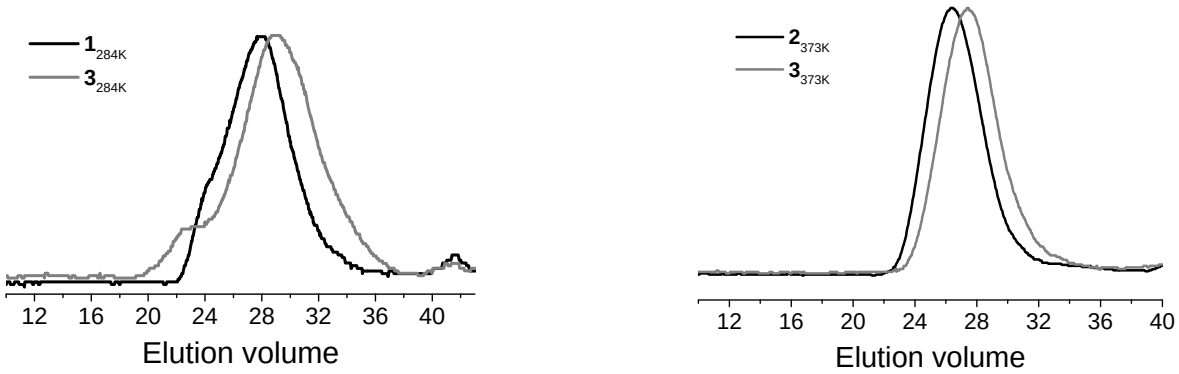

(a) **(b)**

Figure S2 GPC traces of (a) **1** (black) and its derivative **3** (grey) and (b) **2** (black) and its derivative **3** (grey).

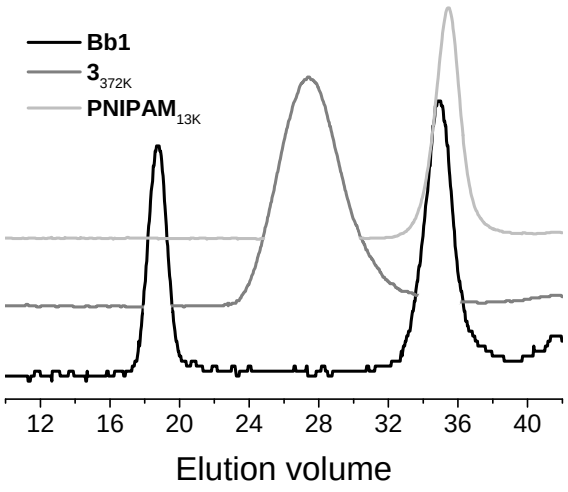

Figure S3 GPC traces of **Bb1** (black), **3** backbone (grey) and **PNIPAM**$_{13K}$ (light grey). The trace of the molecular bottlebrush does not show any peak at the retention volume of the backbone. Un-reacted side chains, however are still present.

ATR-FTIR of 3 (wavenumbers (cm^{-1})):

3086 (C−H stretching vibration for ferrocene), 2931 and 2870 (asymmetric and symmetric C−H stretching vibration in –CH_2–), 2088 (azide), 1447, 1420 (C=C stretching vibration from ferrocene), 1380 (asymmetric deformation vibration of –CH_3 group on Si), 1360 and 1247 (symmetric –CH_3 deformation vibration), 1160 (asymmetric ring in-plane vibration for ferrocene), 1034 (asymmetric ring out-of-plane vibration for ferrocene), 892 (–CH_3 rocking vibration in Si−CH_3), 865 (Si−C stretching vibration), 826 (in-plane C−H stretching in ferrocene), 771 and 742 (out-of-plane C−H deformation in ferrocene).

ATR-FTIR PNIPAM$_{13K}$ by ATRP 1a (wavenumbers (cm^{-1})):

3289 (N-H symmetric and asymmetric stretching vibration), 3078, 2971, 2933, 2874 (asymmetric and symmetric C−H stretching vibration in -CH_2-), 1635 (C=O stretching vibration), 1535 (amide II), 1458, 1386, 1366, 1170

ATR-FTIR of Bb1,Bb2,Bb3 (wavenumbers (cm^{-1})):

3289 (N-H symmetric and asymmetric stretching vibration), 3078, 2971, 2933, 2874 (asymmetric and symmetric C−H stretching vibration in -CH_2-), 1635 (C=O stretching vibration), 1535 (amide II), 1458, 1386, 1366, 1170, 1037 (asymmetric ring-out-of-plane vibration for ferrocene).

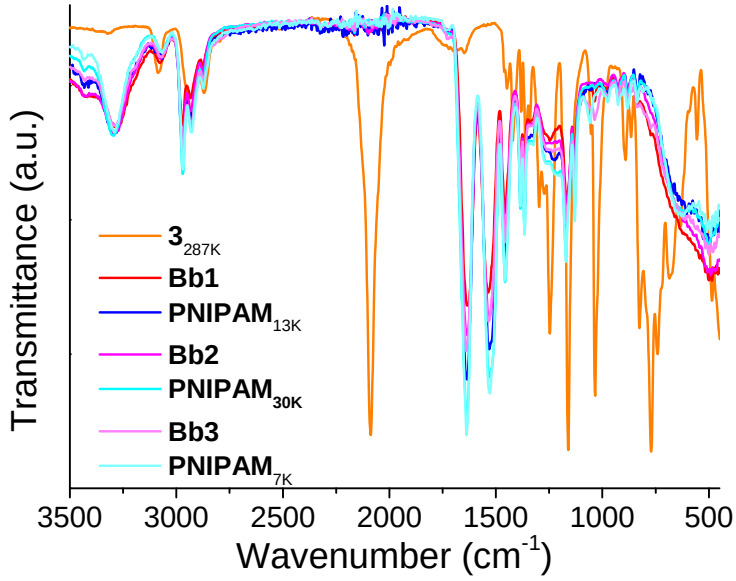

(a)

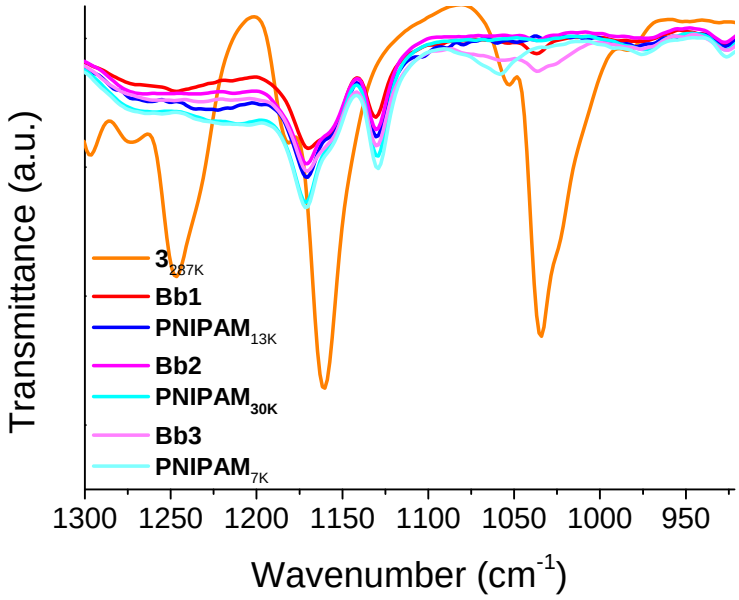

(b)

Figure S4 (a) ATR-FTIR spectra of the molecular bottlebrushes. As a comparison, spectra of **3** and the three PNIPAM side chains are included. The completion of the click reaction is apparent from the absence of the azide stretching peak at 2088 cm^{-1}. (b) Magnification of (a) between 1300 and 900 cm^{-1}, each bottlebrush has a peak at 1036 cm^{-1} belonging to the out–of–plane vibration of the ferrocene rings.

2 Synthesis of grBb

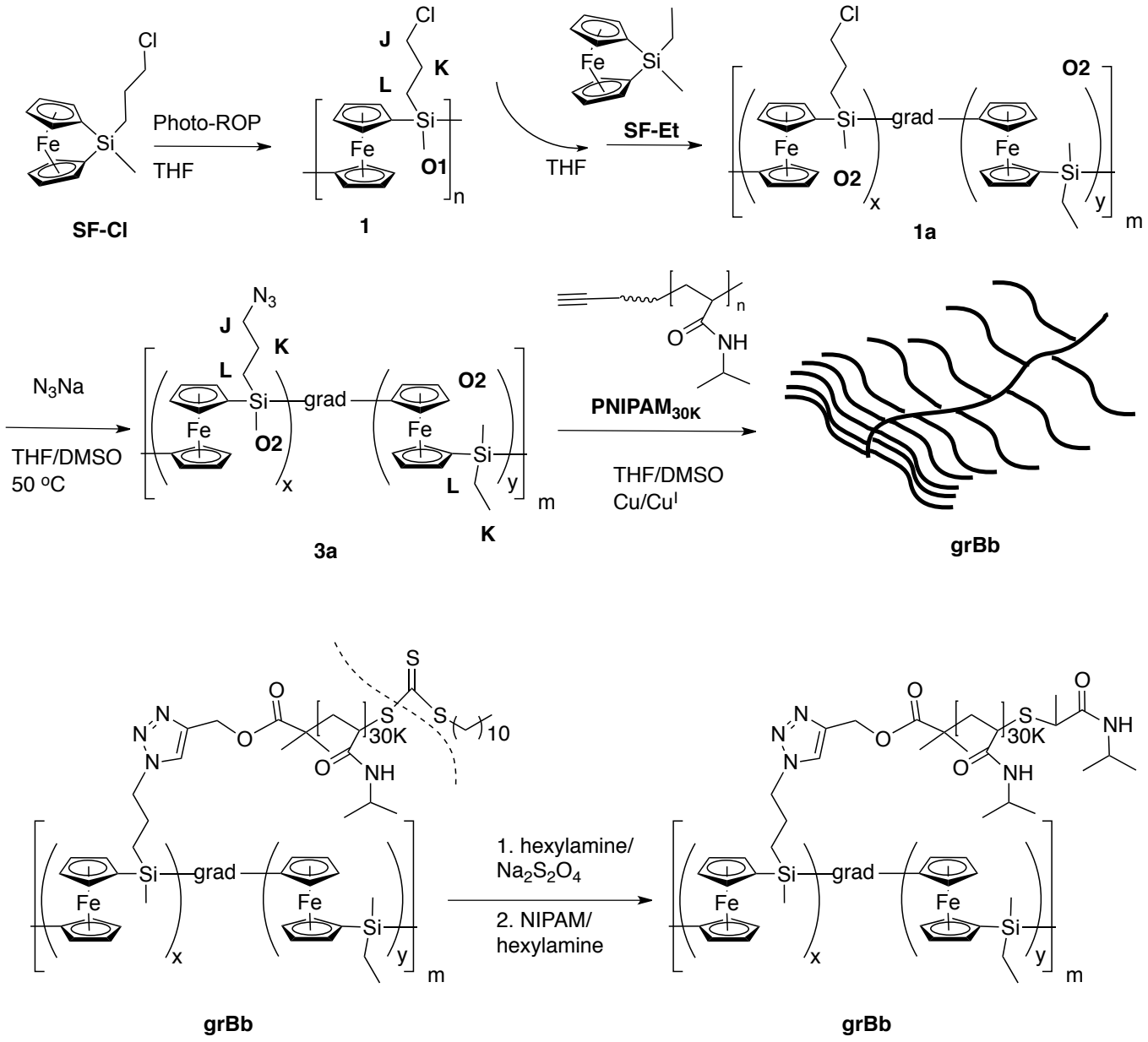

Scheme S2 Synthesis of gradient bottlebrush (**grBb**) via click chemistry.

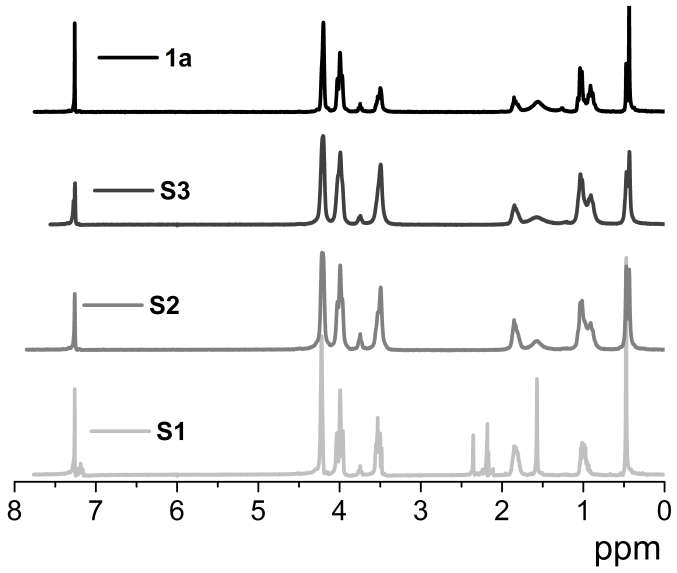

(a)

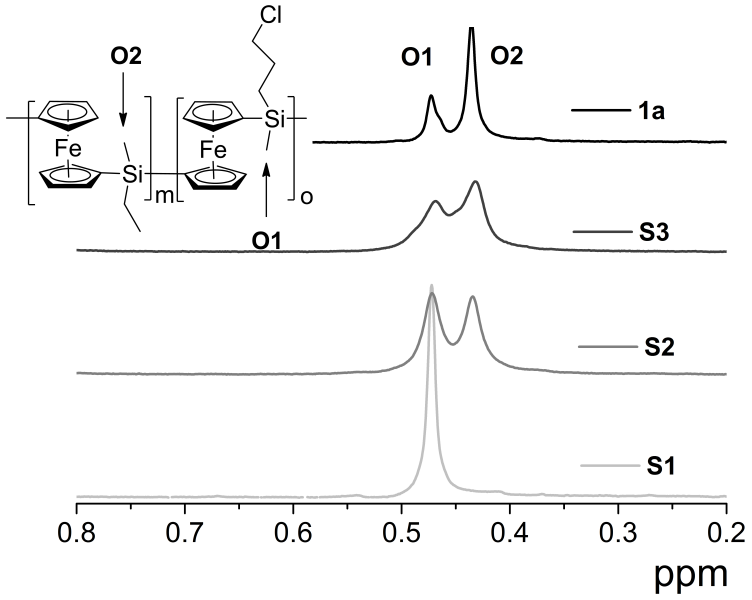

(b)

Figure S5 ^{1}H NMR spectra of samples *S1–S4* from bottom to top taken during gradient colopymerization, the magnified part shows the ratio of the two different repeat units in the PFS chain.

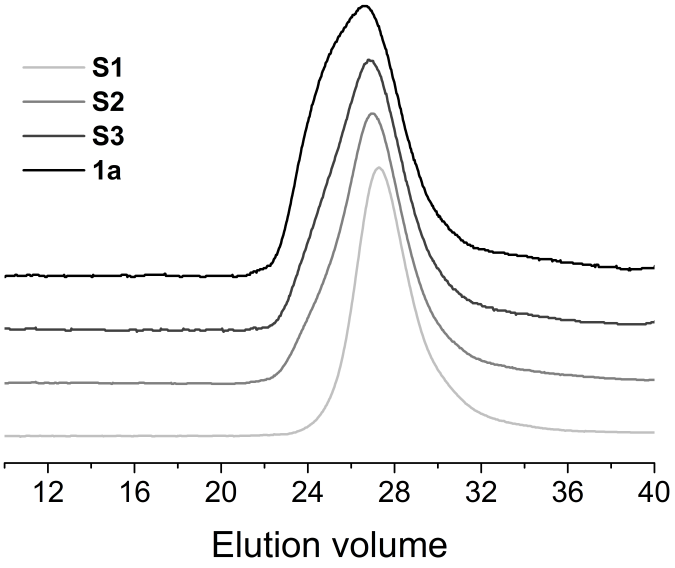

Figure S6 GPC traces of samples taken during the formation of gradient PFS. The peaks shift to lower elution volumes as the polymerization proceeds.

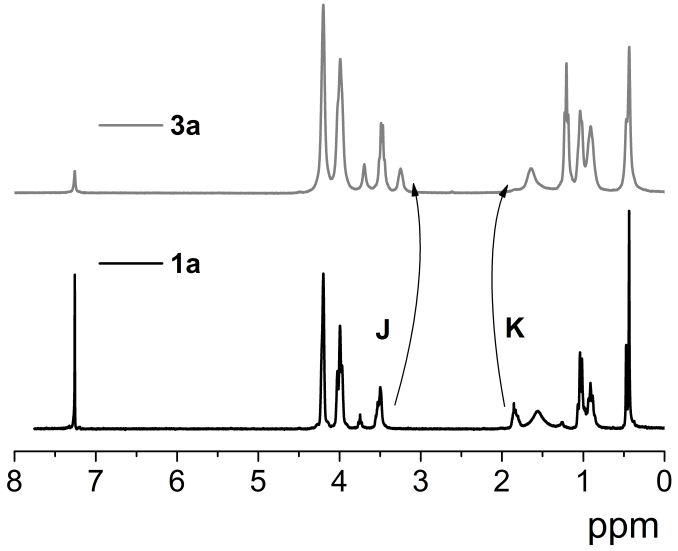

(a)

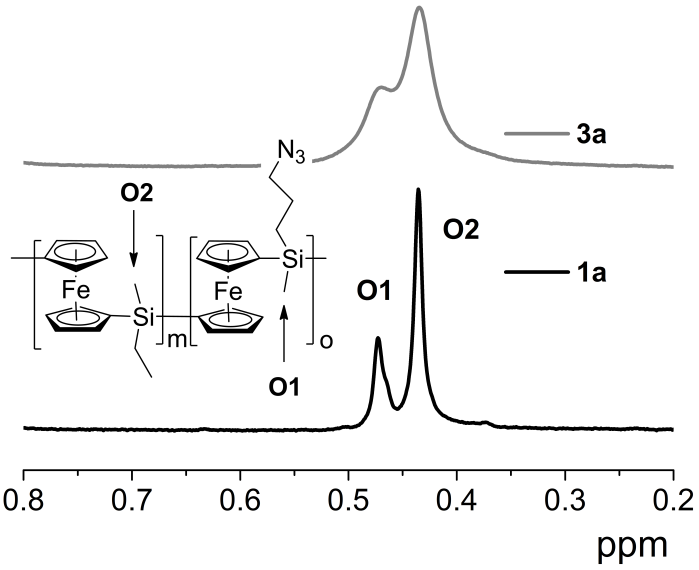

(b)

Figure S7 ^{1}H NMR spectrum of **1a** and **3a**. The conversion of the side group is evident from the shift of the peaks belonging to the pendant groups attached to Si. For guidance to the symbols **J** and **K** see Scheme S2.

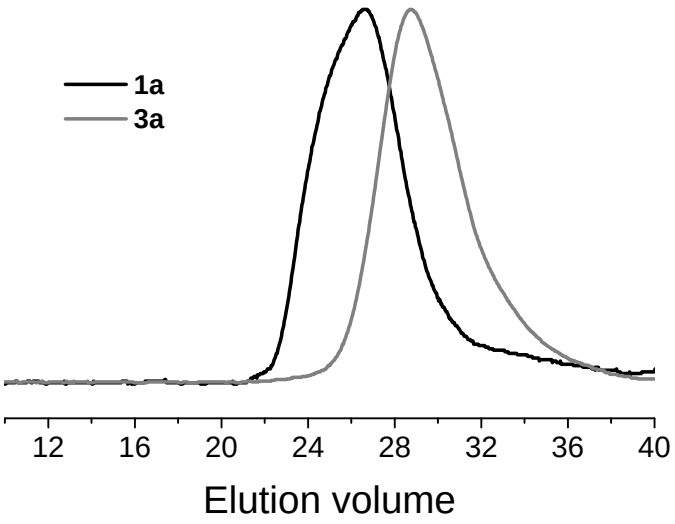

Figure S8 GPC traces of **1a** (black) and its derivative **3a** (grey).

ATR-FTIR of 1a (wavenumbers (cm^{-1})):

3086 (C−H stretching vibration for ferrocene), 2931 and 2870 (asymmetric and symmetric C−H stretching vibration in $–CH_2–$), 1447, 1420 (C=C stretching vibration from ferrocene), 1380 (asymmetric deformation vibration of $–CH_3$ group on Si), 1360 and 1247 (symmetric $–CH_3$ deformation vibration), 1160 (asymmetric ring in-plane vibration for ferrocene), 1034 (asymmetric ring out-of-plane vibration for ferrocene), 892 ($–CH_3$ rocking vibration in $Si–CH_3$), 865 (Si−C stretching vibration), 826 (in-plane C−H stretching in ferrocene), 771 and 742 (out-of-plane C−H deformation in ferrocene).

ATR-FTIR of 3a (wavenumbers (cm^{-1})):

3086 (C−H stretching vibration for ferrocene), 2931 and 2870 (asymmetric and symmetric C−H stretching vibration in $–CH_2–$), 2088 (azide), 1447, 1420 (C=C stretching vibration from ferrocene), 1380 (asymmetric deformation vibration of $–CH_3$ group on Si), 1360 and 1247 (symmetric $–CH_3$ deformation vibration), 1160 (asymmetric ring in-plane vibration for ferrocene), 1034 (asymmetric ring out-of-plane vibration for ferrocene), 892 ($–CH_3$ rocking vibration in $Si–CH_3$), 865 (Si−C stretching vibration), 826 (in-plane C−H stretching in ferrocene), 771 and 742 (out-of-plane C−H deformation in ferrocene).

ATR-FTIR of grBb (wavenumbers (cm^{-1})):

3289 (N-H symmetric and asymmetric stretching vibration), 3078, 2971 and 2933 and 2874 (asymmetric and symmetric C−H stretching vibration in $–CH_2–$), 1635 (C=O stretching vibration), 1535 (amide II), 1458, 1386, 1366, 1170, 1037 (asymmetric ring- out-of-plane vibration for ferrocene).

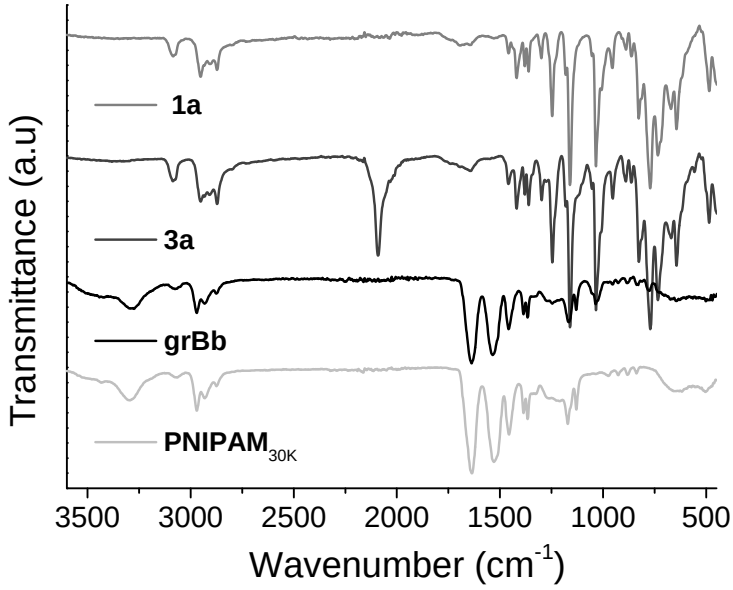

(a)

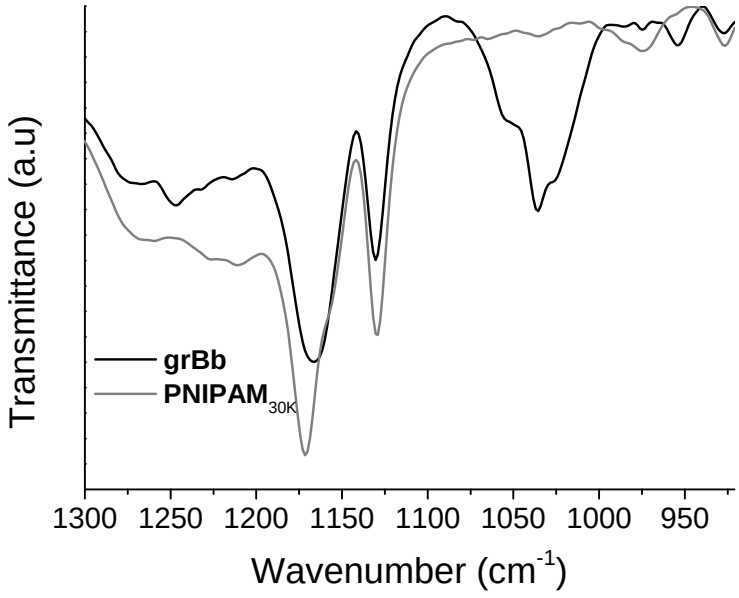

(b)

Figure S9 (a) ATR-FTIR spectra of the **grBb**, **1a**, **3a** and the alkyne-bearing **PNIPAM**$_{30K}$. The completion of the click reaction is apparent from the absence of the azide stretching peak at 2088 cm^{-1} in the spectrum of **grBb**. (b) Magnification of (a) the region between 1300 and 900 cm^{-1}, the absorbance at 1036 cm^{-1} in the spectrum of **grBb** belonging to the out-of-plane vibration of the ferrocene rings, is absent from the spectrum of **PNIPAM**$_{30K}$.

3 Synthesis of Bb4

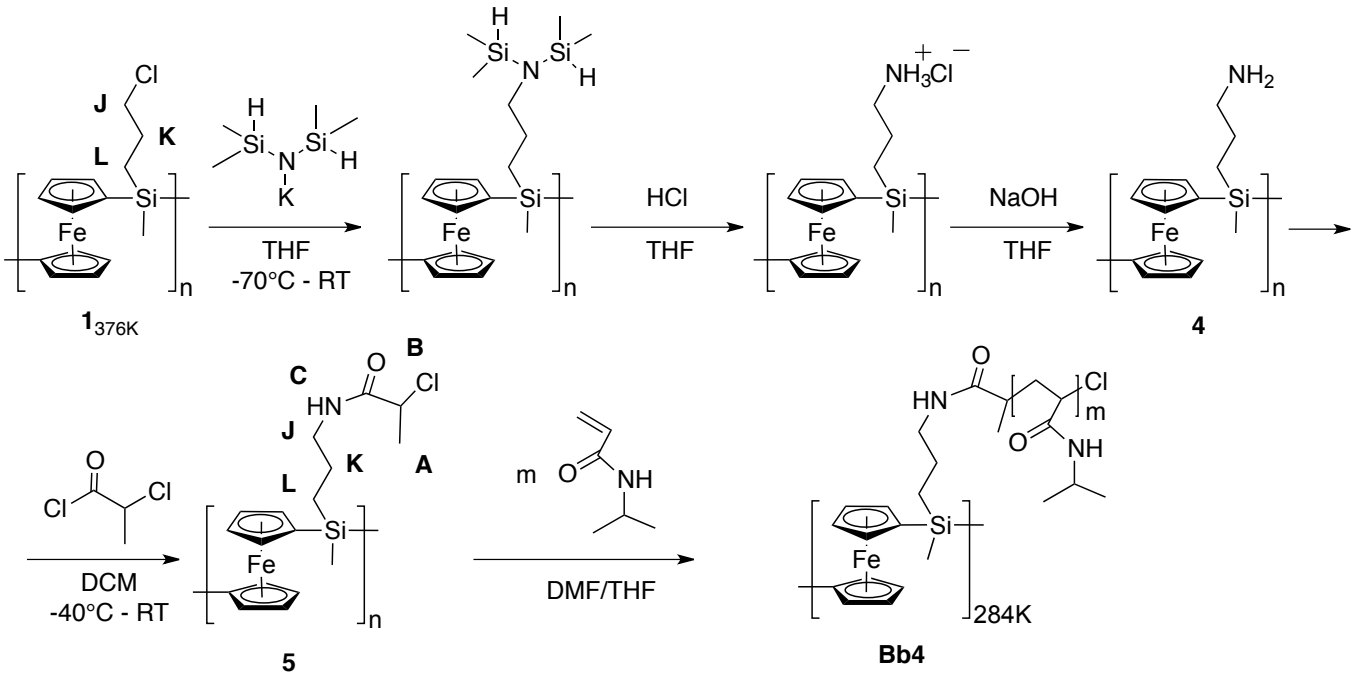

Scheme S3 Synthesis of bottlebrush (**Bb4**) via a grafting from approach by ATRP.

ATR-FTIR of 5 (wavenumbers (cm^{-1})):

3290 (N-H symmetric and asymmetric stretching vibration), 3083 (C−H stretching vibration for ferrocene), 2949, 2870 (asymmetric and symmetric C−H stretching vibration in -CH_2-), 1655 (C=O stretching vibration), 1528 (amide II), 1441 (from PFS), 1420 (C=C stretching vibration from ferrocene), 1379 (asymmetric deformation vibration of –CH_3 group on Si), 1362, 1247 (symmetric –CH_3 deformation vibration), 1161 (asymmetric ring in-plane vibration for ferrocene), 1035 (asymmetric ring- out-of-plane vibration for ferrocene), 909, 892, 865 (Si−C stretching vibration), 828 (in-plane C−H stretching in ferrocene), 772 (out-of-plane C−H deformation in ferrocene).

ATR-FTIR of Bb4 (wavenumbers (cm^{-1})):

3291 (N−H symmetrical/asymmetrical stretching vibration), 3078, 2967, 2926, 2872 (asymmetric and symmetric C−H stretching vibration in –CH_2–) 1638 (C=O stretching vibration), 1532 (amide II), 1456, (–CH_2– scissor vibration), 1385, 1365, 1171, 1036 (asymmetric ring-out-of-plane vibration for ferrocene).

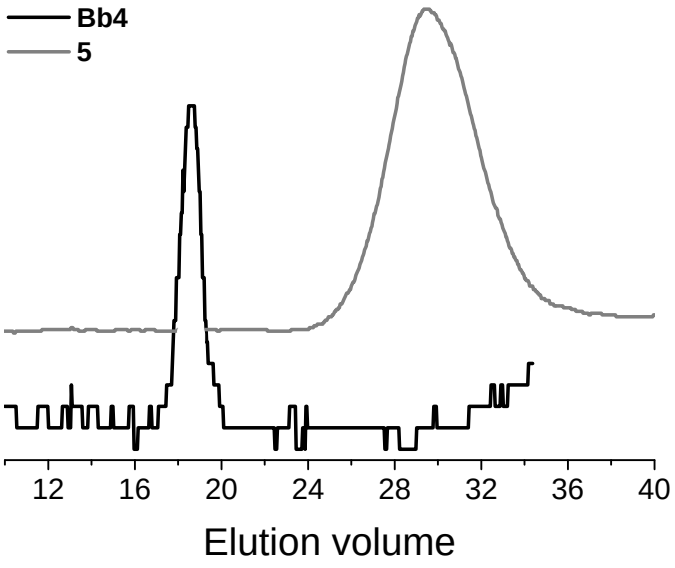

Figure S10 GPC traces of **Bb4** (black) and its macroinitiator: **5** (grey).

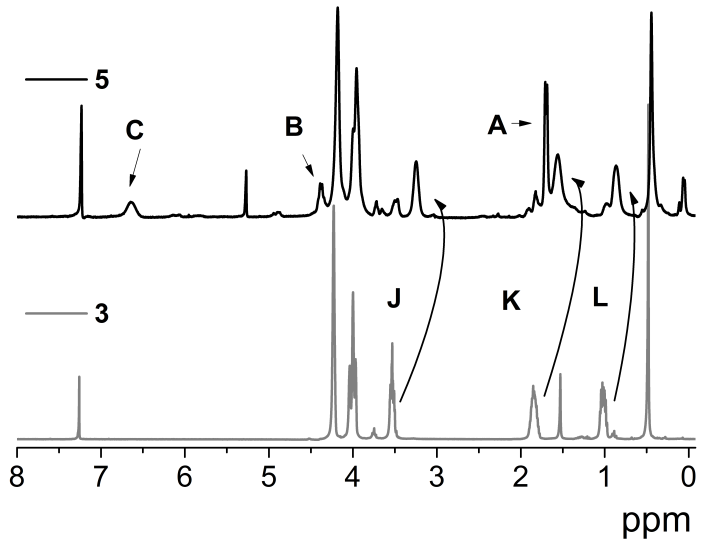

(a)

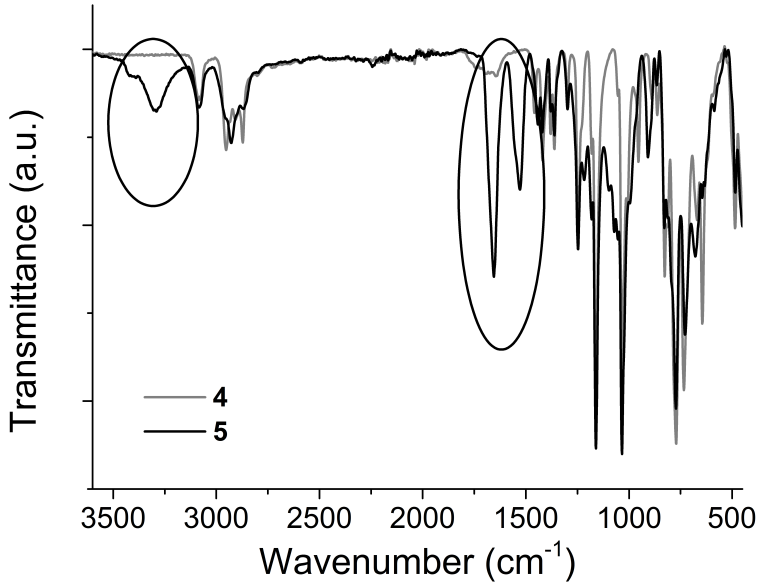

(b)

Figure S11 (a) ^{1}H NMR spectrum of **5**. The completion of the reaction can be followed by the shift of the peaks: **L** shifts from δ = 1 to 0.9 ppm, **K** from δ = 1.8 to 1.6 ppm while **J** shifts from δ = 3.5 to 3.2 ppm, **B** of the initiator moiety appears at δ = 4.4 and **C** at δ = 6.6 ppm. (b) ATR-FTIR spectrum of **5**, the appearance of the characteristic amide peaks indicates the completion of the reaction: Amide I at 3290, 1655 and Amide II at 1528 cm^{-1}. For guidance to the symbols **A**, **B**, **C**, **J**, **K** and **L** see Scheme S3.

4 Thermogravimetric analysis of grafted to bottlebrushes

Thermogravimetric analysis

Isothermal weight loss of the polymer samples (5–10 mg) was measured under N_2 environment (flow rate 20 ml/min) as a function of time for different temperatures with a Perkin–Elmer thermogravimetric analyzer (Pyris 1, Waltham, Ma, USA). The temperature was stepped between 50–600 ° with a rate of 10 °/min.

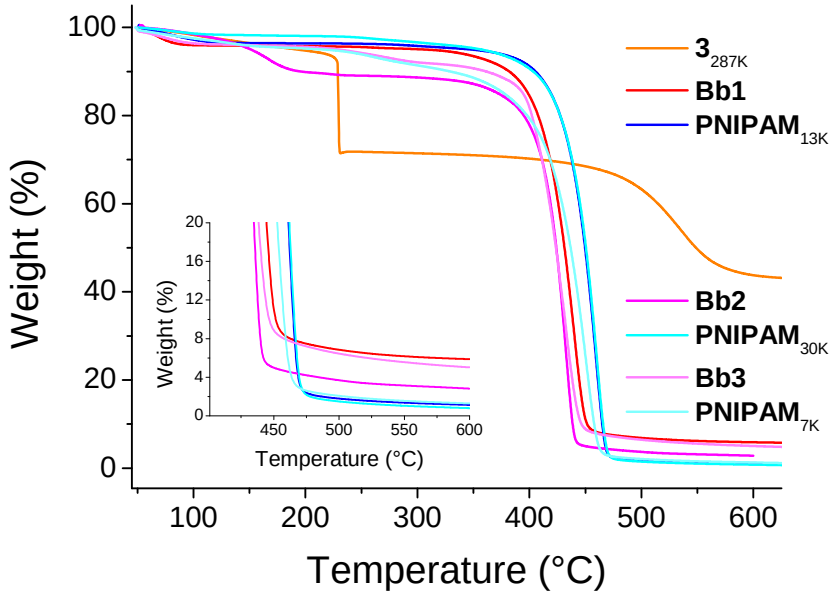

Figure S12 Thermogravimetric analysis of the bottlebrush molecules. As a reference PFS–N_3 and the three PNIPAM side chains are shown. The inset presents a magnification of the region between 400 and 600 °C.

Thermogravimetric analysis of the obtained bottlebrush molecules supports the result of the previously mentioned measurements (Figure S12). The decomposition patterns of $\mathbf{3}_{287}$ and **PNIPAMs** are clearly different. **PNIPAMs** were stable up to 350–400 °C depending on the molar mass of the polymer, and left a low residual weight. $\mathbf{PNIPAM}_7$ displayed two decomposition steps. At 250 °C the polymer lost 5% weight and decomposed at 380 °C, leaving a residual weight of 1.4%. $\mathbf{PNIPAM}_{13}$ and $\mathbf{PNIPAM}_{30}$ were stable up to 380 °C and after decomposition, 1.0 and 0.6 wt.% remained, respectively. The bottlebrush molecules followed a similar decomposition path as PNIPAM, but resulting in a higher residual weight. **Bb2** decomposed in two steps, losing 5% weight at 150 °C, and at 345 °C finally resulting in the lowest residual weight (2.8 wt.%). Indeed, **Bb2** had the largest amount of PNIPAM. **Bb3** decomposed at 345 °C resulting in 5% residual weight, while the less PNIPAM containing bottlebrush **Bb1** left 5.9 % weight upon decomposition at 345 °C. **grBb** decomposed in two steps, losing 5-10 wt.% at 150 °C and most of its weight at 350 °C, resulting in 5.6% residual weight. Decomposition of $\mathbf{3}_{287}$ occured at 250 °C and the 43% residual weight originates from the remaining iron and silicon, which are responsible for the residual weight of the bottlebrushes as well.

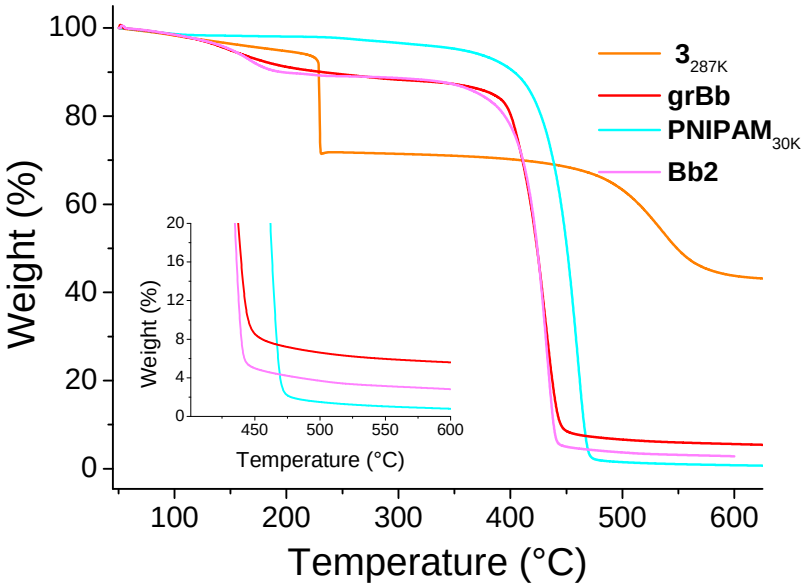

Figure S13 Thermal decomposition of the **grBb** molecule, as a reference **PFS-N$_3$**, the **PNIPAM** side chain and **Bb2** are shown. The inset is a magnification between 400 and 600 °C.

5 Static light scattering

Static light scattering of aqueous bottlebrush solutions measurements were performed on an ALV instrument equipped with a 300 mW Cobolt Samba-300 DPSS laser operating at a wavelength of 532 nm. The samples were contained in glass cells with a diameter of 1.5 cm, and thermostated to 20 °C. The detector was stepped between 20 and 110 ° at every 5°, and scattering intensities were collected four times for 20 sec. The parallel measurements were averaged. The data was analysed according to the literature[1], corresponding Zimm diagrams are plotted in Figure S14. The dn/dc was determined using a Brice-Phoenix refractometer (Phoenix Precision Instrument co.), equipped with filters and a mercury-vapor lamp as a light source. The dn/dc (for the bottlebrushes) was found to be 0.145 mL/g in water at 24 °C.

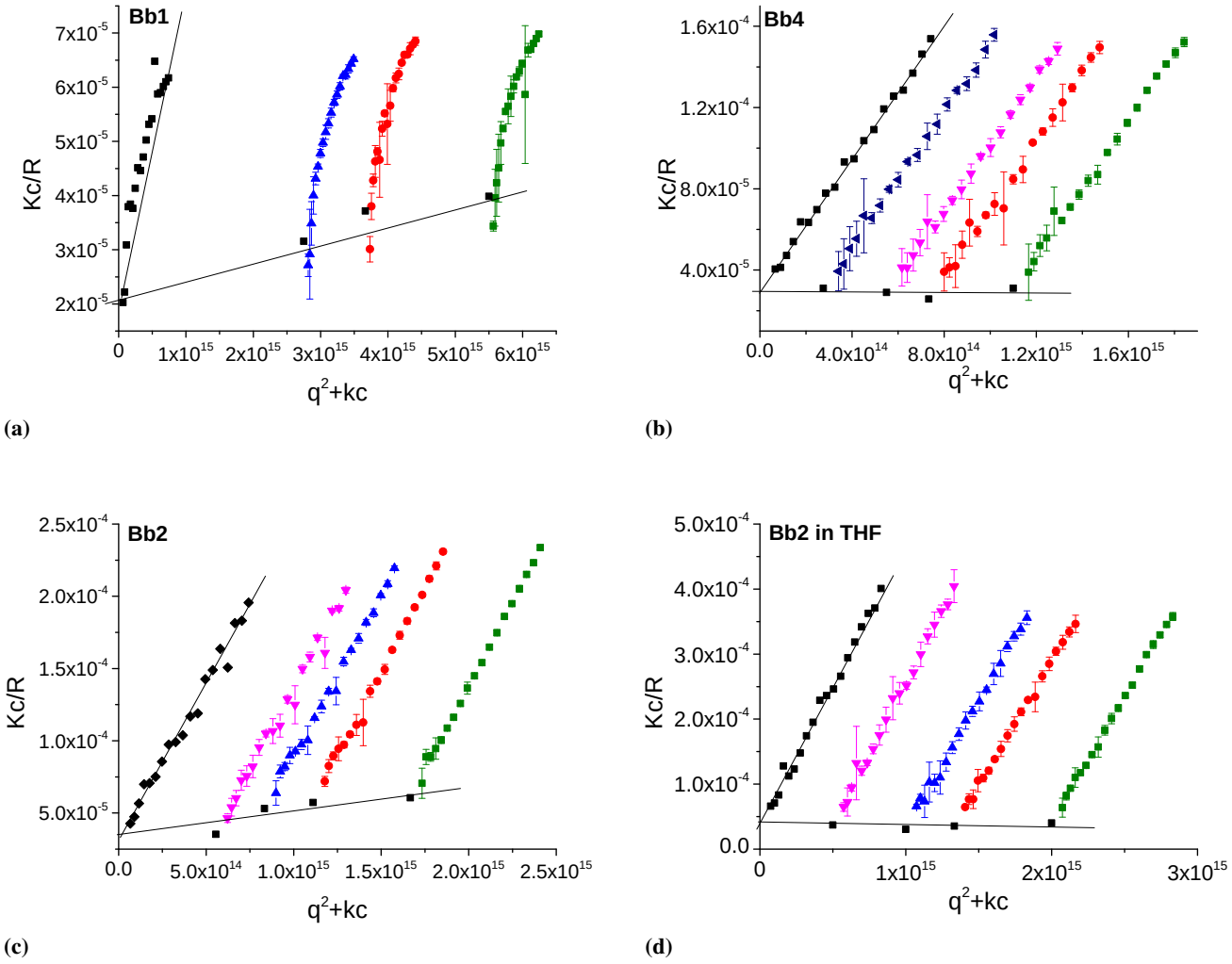

Figure S14 Zimm diagrams constructed from the static light scattering

The obtained fitted values are summarized in Table 1. The SLS data shows no aggregation of the bottlebrushes, since after dilution of the solutions the scattering intensities scale accordingly. The obtained

sizes (R_g) imply the presence of huge molecules with molar mass (M_w) values of 10-20 million g/mol, however, this is not expected from the calculations based on NMR and GPC spectra. Since the basic SLS theory is valid for linear polymer chains, deviations may occur when more compact, branched structures are studied. Molar masses obtained here by SLS may therefore not represent the true molar mass values of the bottlebrush polymers.

Table 1 Molecular characteristics obtained from the SLS measurement.

	R_g (nm)	M_w (10^6 g/mol)	B_2 (m^3/mol)
Bb1	83	39.9	111592
Bb4	129	33.9	-2029
Bb2	146	32.7	107690
Bb2 THF	203	31.2	14666

6 Electrochemistry

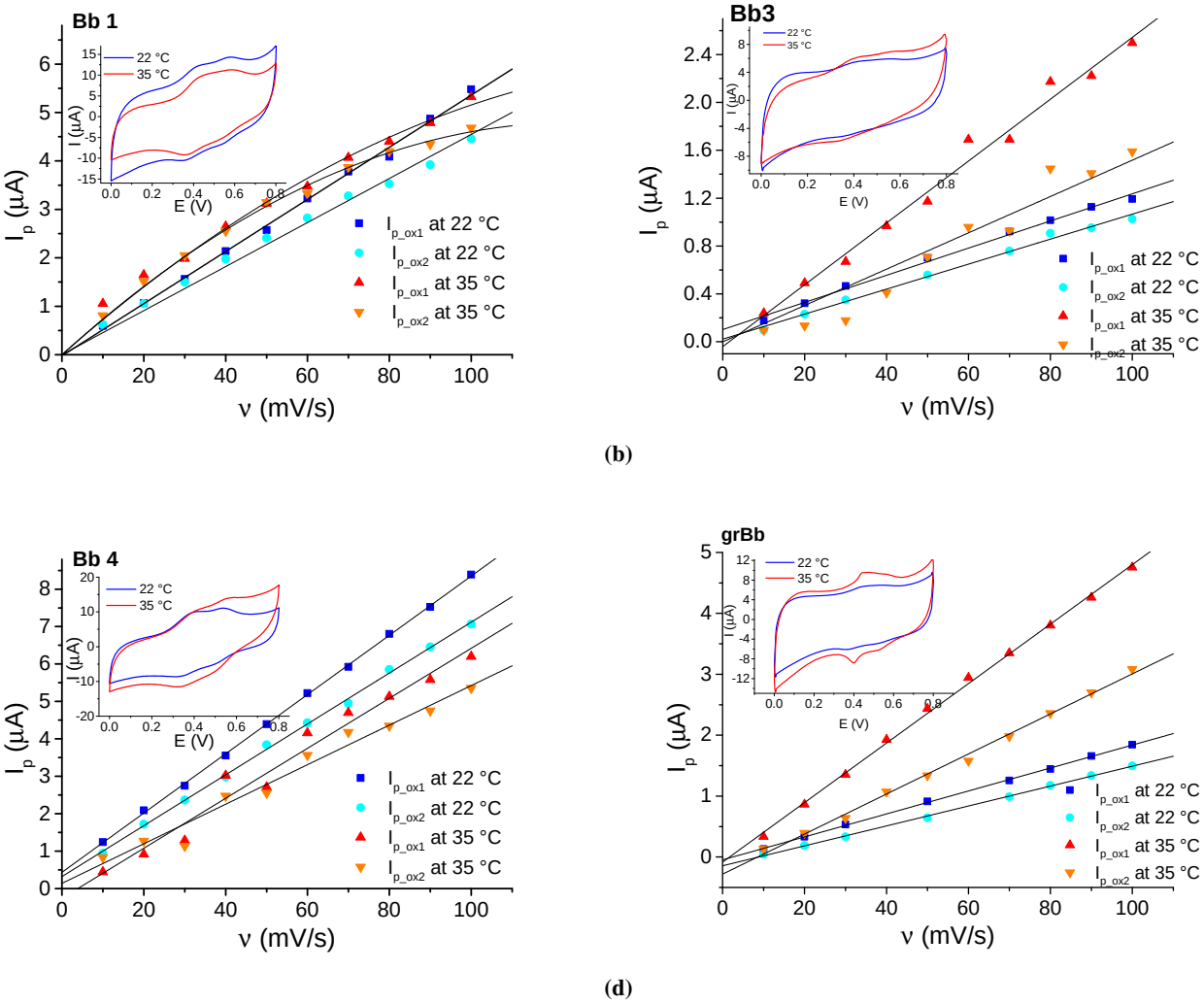

Figure S15 Dependence of peak currents versus scan rates of (a) **Bb1**, (b) **Bb1**, (c) **Bb4** and (d) **grBb** adsorbed on HOPG electrode. Reference electrode Ag/AgCl, counter electrode Pt, 0.1 M aqueous $NaClO_4$. Insets show the cyclic voltammograms recorded at a scan rate of 50 mV/s.

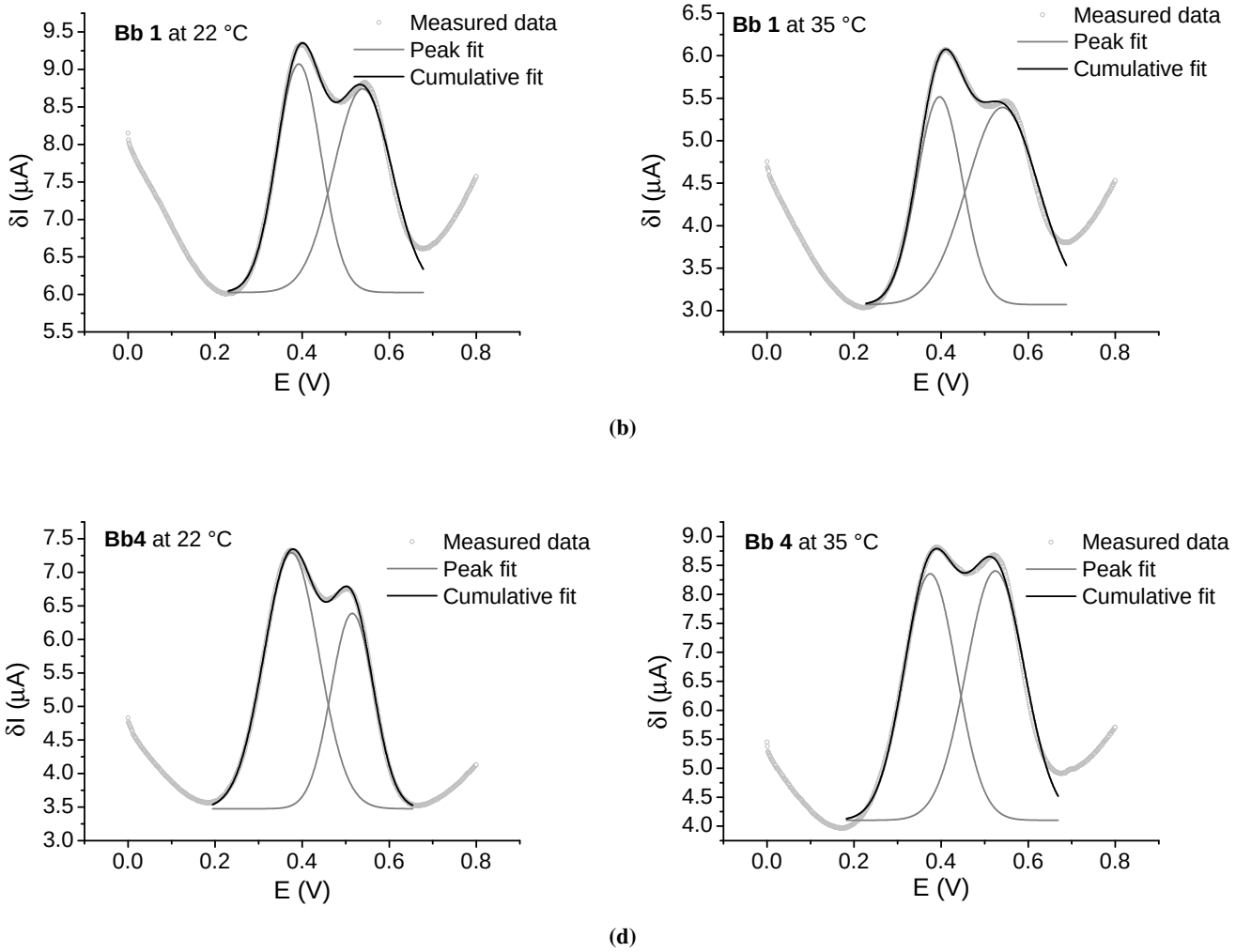

Figure S16 Differential pulse voltammogram recorded of **Bb1**: (a) at 22 °C (b) 35 °C and **Bb4**: (c) at 22 °C (d) 35 °, adsorbed on HOPG (v = 5 mV/s scan rate, 50 ms pulse time, 200 ms interval time, 10 mV pulse height reference electrode Ag/AgCl, counter electrode Pt, 0.1 M aqueous $NaClO_4$.

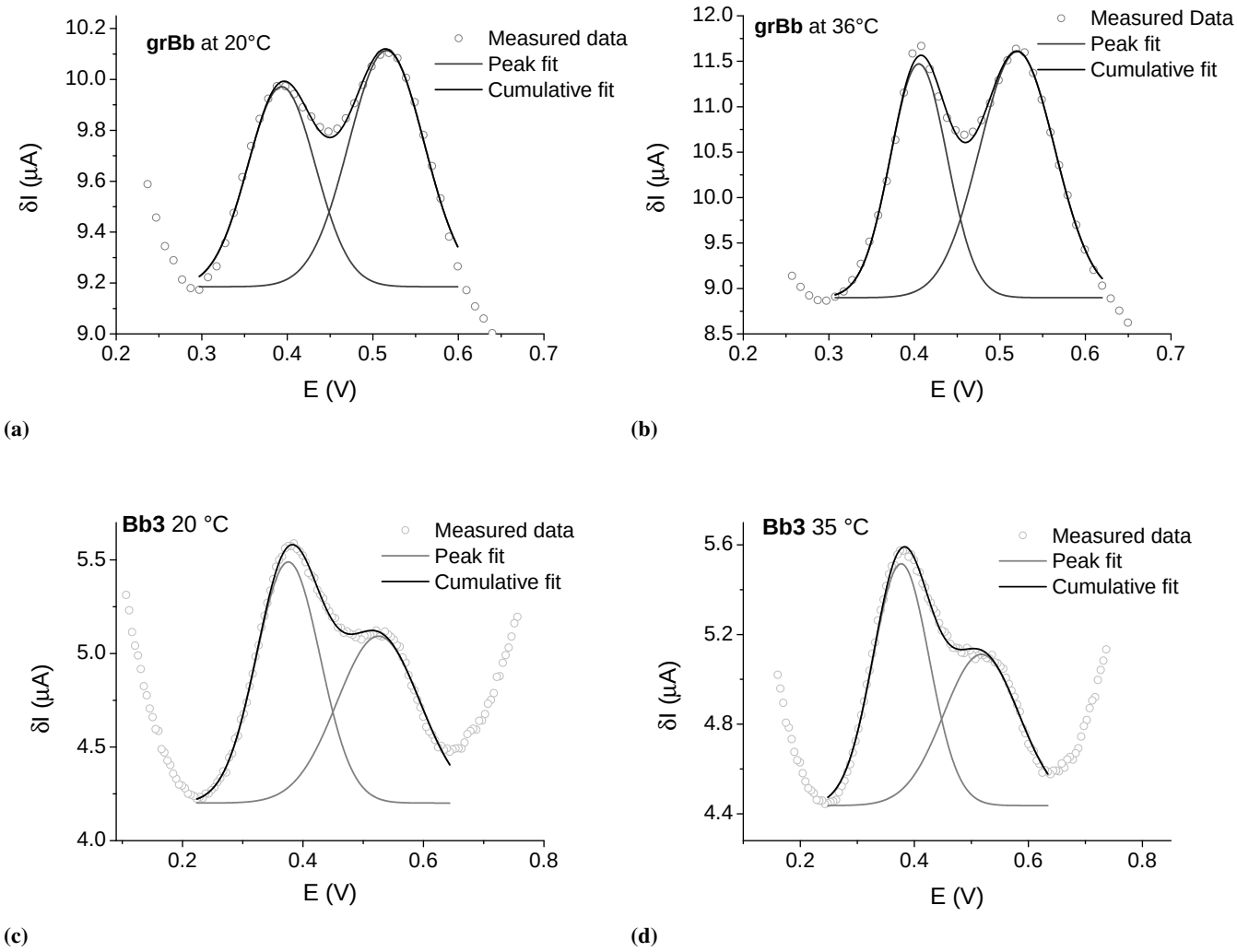

Figure S17 Differential pulse voltammogram recorded of **grBb**: (a) at 22 °C (b) 36 °C, and **Bb3**: (a) at 22 °C (b) 35 °C adsorbed on HOPG (ν = 5 mV/s scan rate, 50 ms pulse time, 200 ms interval time, 10 mV pulse height reference electrode Ag/AgCl, counter electrode Pt, 0.1 M aqueous $NaClO_4$.

References

[1] H. M. van der Kooij, E. Spruijt, I. K. Voets, R. Fokkink, M. A. Cohen-Stuart and J. van der Gucht, *Langmuir*, 2012, **28**, 14180–91.